Air-Coupled Lamb Wave Tomography

William Wright, David Hutchins, *Member, IEEE*, Dion Jansen, and David Schindel

***Abstract*—An entirely air-coupled inspection system using a pair of micromachined silicon capacitance transducers has been used to image defects in thin plates of different materials (0.7 mm to 2.22 mm thick) using air-coupled Lamb wave tomography. A filtered back projection algorithm was used in a form of difference tomography to reconstruct images of defects up to 10 mm diameter machined in aluminium and perspex (Plexiglas) plates, as well as in samples of carbon fiber reinforced polymer (CFRP). The technique was able to resolve non-central defects as well as multiple flaws within the scan area. This flexible tomographic system was able to produce images of the change in a variety of different acoustic variables from only one set of experimental data, with success dependent on the size, shape, and location of the defect in the scan area.**

I. Introduction

TOMOGRAPHIC RECONSTRUCTION [1] is a method of imaging by illuminating the object in many different directions in the plane of interest, usually using X-rays or ultrasound. An image is then formed from changes in a physical variable such as signal amplitude or propagation delay occurring in the planar cross section. Examples of applications using ultrasonic tomography are the testing of SiO_2 ingots [2], solid propellant rocket motors [3], and wooden poles [4]. Perhaps one of the most restricting factors is the volume of data which must be taken. Previous work has automated this process using scanned transducers [5] and transducer arrays [6],[7]. With the advent of non-contact transduction techniques and new composite materials, there has been a resurgence in the application of ultrasonic tomography to non destructive testing [8]–[11]. Recent advances in high-frequency air-coupled ultrasonic transducers [12]–[15] mean that tomography in solid materials using air-coupled ultrasound is now possible, as will be demonstrated in this work.

There are two main groups of tomographic image reconstruction algorithms. Series expansion methods which use iteration [16], such as ART [17] and SIRT [18], can correct for anisotropy [19], ray bending, and non standard sampling geometry but are computationally inefficient. Transform methods [20], such as Fourier inversion [21] and filtered back projection [22],[23], use Fourier analysis and are fast and efficient but require precise sampling geometry. Other techniques use time-of-flight diffraction tomography (TOFDT) [24], filtered back propagation [25], and scattering area functions [26]. This paper will describe how a filtered back projection algorithm used leaky Lamb waves to reconstruct tomographic images of defects in thin sheets of a variety of materials, using a pair of micromachined capacitance transducers in an entirely air-coupled system.

Manuscript received December 28, 1995; revised and accepted June 19, 1996.

W. M. D. Wright and D. A. Hutchins are with the Department of Engineering, University of Warwick, Coventry CV4 7AL, UK.

D. P. Jansen and D. W. Schindel are with the Department of Physics, Queens University, Kingston, Ontario K7L 3N6, Canada.

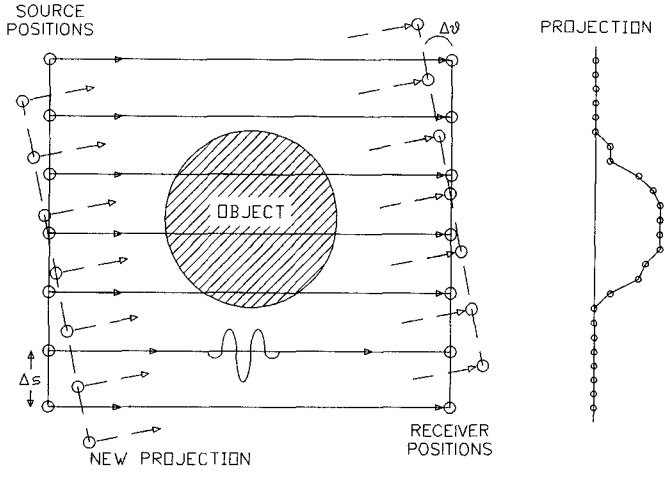

Fig. 1. Schematic diagram of the sampling geometry.

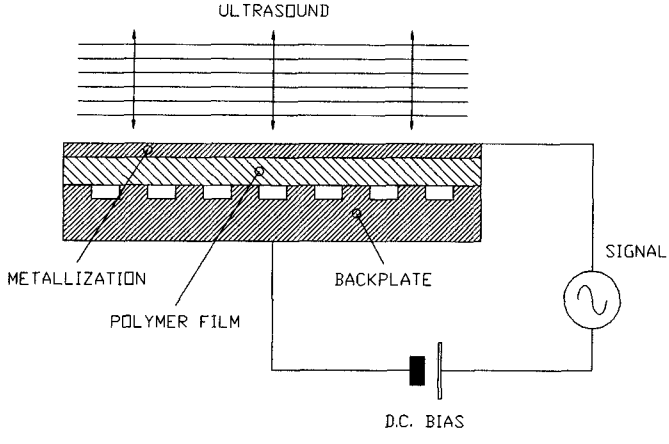

Fig. 2. Schematic diagram showing the construction of a micromachined silicon air-coupled transducer.

II. The Filtered Back Project Theorem

The technique may be explained by considering the sampling geometry shown schematically in Fig. 1, where an ultrasonic source and receiver a fixed distance apart are scanned in one direction over the object to be imaged, and a waveform is taken at regularly spaced intervals Δs. The time of arrival is extracted from each waveform or 'ray,' and this forms one point on a "silhouette" or projection

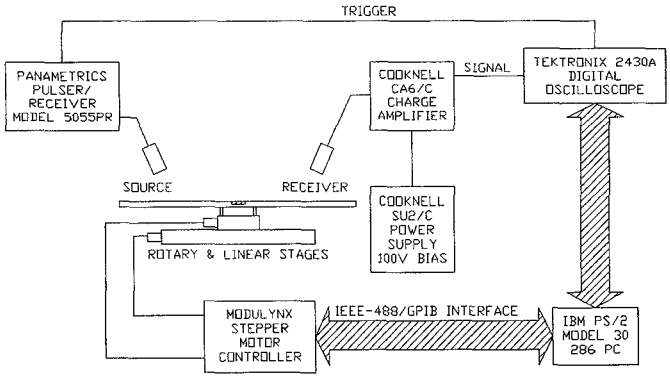

Fig. 3. Schematic diagram of experimental apparatus using a pair of capacitance transducers for an entirely air-coupled system.

through the object. Assuming the ray path is linear, the time of arrival for each waveform is in fact the integral of all the variations in slowness (the inverse of velocity) in a direct line between the source and receiver. We rotate the object or transducer pair through a small angle $\Delta\theta$ and repeat the scanning process until a full 180° has been turned, building up a series of projections of the slowness function arranged through the center of the object like the spokes of a wheel. These projections are then used by the filtered back projection algorithm to reconstruct a 2-dimensional cross-sectional image of all the slowness variations everywhere within the scan area. Although described in terms of times of arrival and slowness function, the technique is the same for any acoustic variable such as attenuation or frequency shift.

The projection theorem states that the 1-dimensional Fourier transform of a projection at an angle θ is equal to the two-dimensional Fourier transform of the actual slowness function through the centre of the object at the same angle θ. By substitution and manipulation, the 2-dimensional Fourier transform simplifies to a back projection of all these projections, convolved with a kernel function in the Fourier domain, which is a simple filtering operation. For a more detailed description of the theorem used in this work, see reference [23].

Riemann approximations were used as the waveforms were taken at evenly spaced intervals over equally spaced angular projections through 180°. As the points in the back projection did not exactly match the positions of the data points in each convolved projection, linear interpolation was used to accurately obtain the slowness function at any point in the scan area. The frequency bandwidth of the convolutions in the Fourier domain are limited by the Nyquist theorem, given by

$$B = \frac{1}{2\Delta s} \tag{1}$$

where B is the bandwidth, and Δs is the linear spacing of each ray. The highest spatial frequency S_0 is given by

$$\Delta s \leq \frac{1}{2S_0} \tag{2}$$

To reduce high frequency introduced by the kernel function, a low pass filter or window function is included in the convolution stage, with the frequency limit set at the Nyquist bandwidth B. In this work, the filter function was a simple Hamming window, which offered the best compromise between inclusion of the higher frequencies and suppression of noise.

III. Equipment and Experimental Technique

The micromachined silicon air-coupled capacitance transducers used in this study are shown schematically in Fig. 2. The devices consisted of a contoured conducting backplate over which metallized Mylar films either 2.5 μm (receiver) or 5 μm (source) thick were placed. The backplate was produced by anisotropically etching an array of pits 40 μm in diameter, 40 μm deep, and 80 μm apart into a silicon wafer, and then coating with gold. The backplate and film formed two electrodes of a capacitor, between which a bias voltage was applied. When the membrane is acting as a transmitter, a transient voltage applied between the two electrodes causes motion of the membrane and the generation of ultrasound in air. When it is used as a receiver, ultrasonic waves in air cause the membrane to move, varying the charge between the two electrodes. The construction and characterisation of these devices is discussed in greater detail in references [14] and [15].

The tomography was performed using the apparatus shown schematically in Fig. 3. In this work, ultrasonic waves were generated in air using a micromachined silicon capacitance transducer driven by a Panametrics pulser-receiver model 5055PR, which delivered a -200 V transient with a rise time of < 10 ns. Waveforms were received by another silicon transducer, connected to a Cooknell CA6/C charge amplifier with a sensitivity of 250 mV/pC which also supplied a 100 V d.c. bias between the two electrodes. Signals were captured using a Tektronix 2430A digital oscilloscope and transferred via an IEEE-488/GPIB interface to an IBM PS/2 model 30286 PC, which was also used to control the linear and rotary Daedal stages using a Modulynx stepper motor controller. The stages were accurate to within ± 0.01 mm. Unless stated otherwise, the dimensions of each scan were 50 mm in steps of 1 mm, giving 51 rays per projection, and 180° in steps of 5°, giving 37 projections.

Conventional tomographic imaging usually requires absolute measurements of arrival time or amplitude along known ray paths. However, using the air coupled transducers, the exact point of generation or reception was not known; also, there were additional delays and attenuation caused by the air gap. To overcome these unknowns, a form of difference tomography was employed in which all measurements were made with respect to the first ray path in each projection. The reconstructed image would then be of the change in a parameter caused by the presence of a defect.

In addition to arrival time and signal amplitude, another useful parameter in determining the presence of a

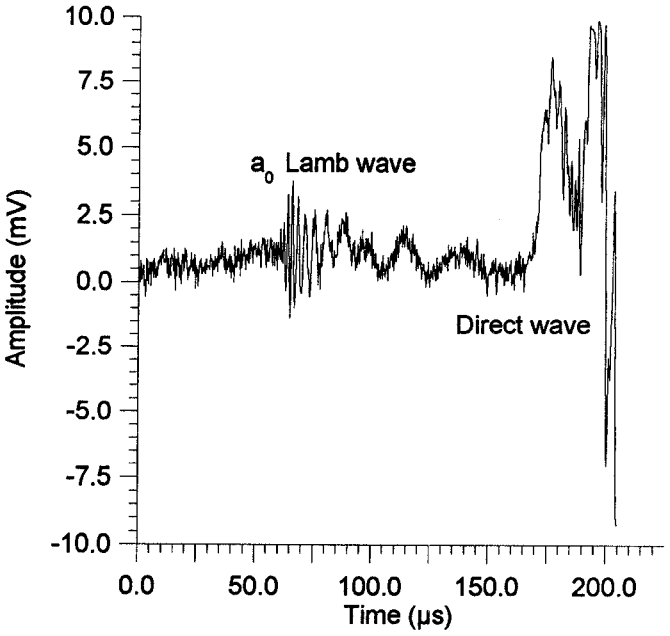

Figure 4(a)

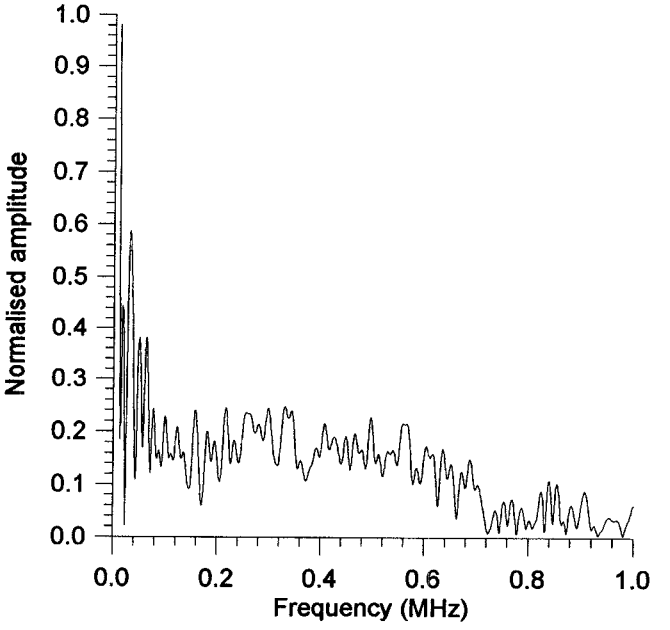

Figure 4(b)

Fig. 4. (a) A typical Lamb wave in a 0.69 mm aluminium sheet, obtained using the pair of air-coupled transducers. (b) The normalized frequency spectrum of Fig. 4(a).

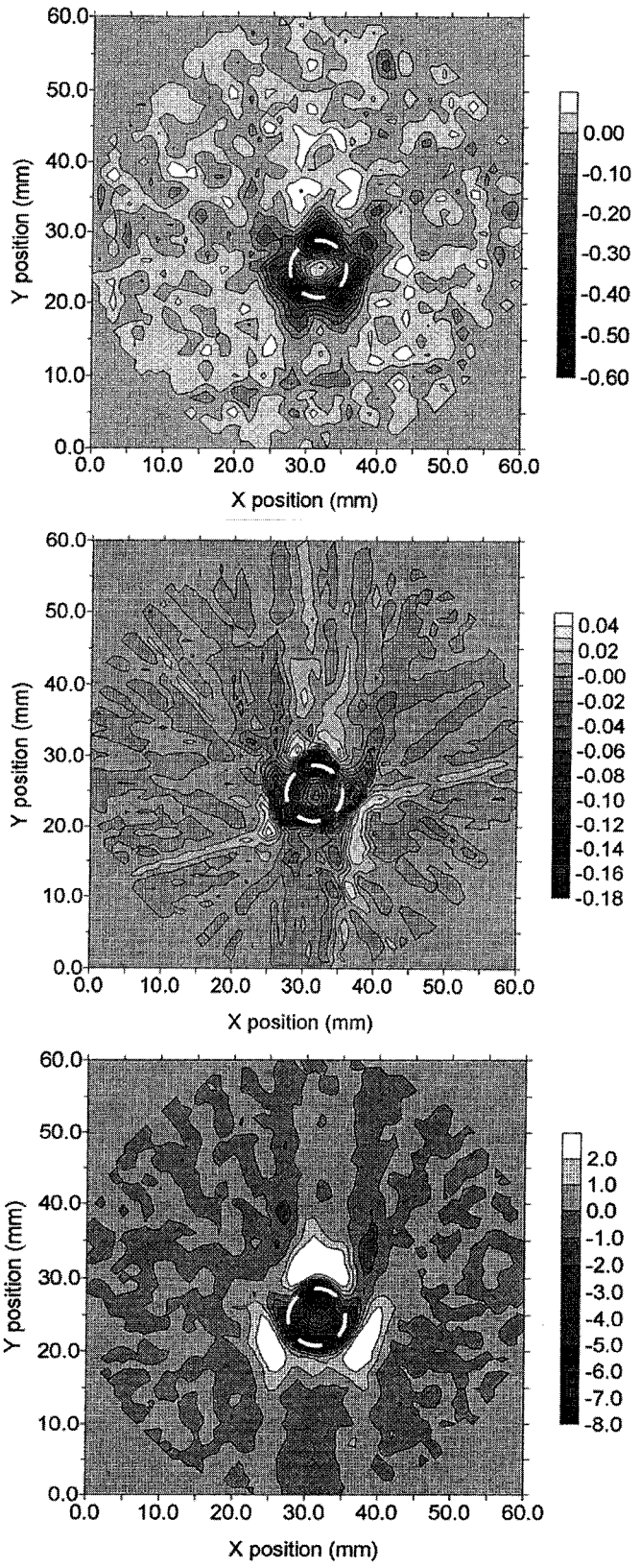

Fig. 5. (a) Attenuation image in dB mm^{-1} of an 8 mm diameter recess machined halfway through a 0.69 mm thick aluminium sheet. (b) Slowness image in μs mm^{-1} for an 8 mm diameter recess machined halfway through a 0.69 mm aluminium sheet. (c) Image of the shift in centroid frequency in kHz for an 8 mm diameter recess machined halfway through a 0.69 mm aluminium sheet.

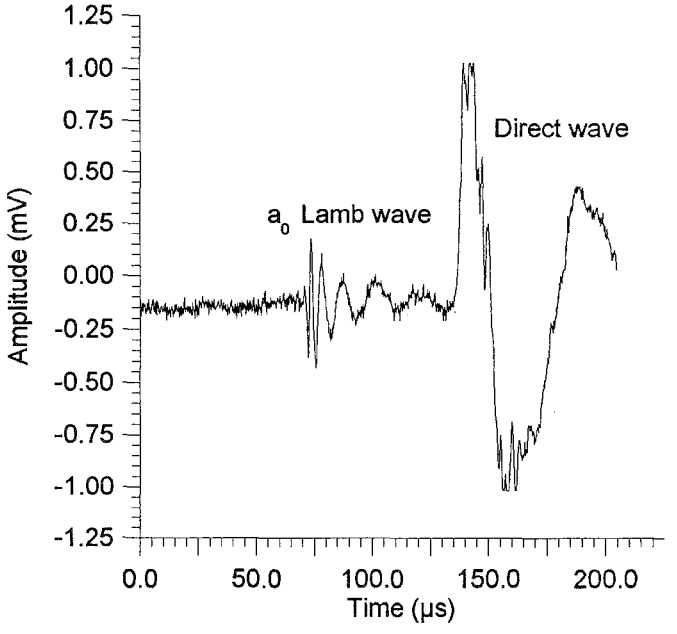

Figure 6(a)

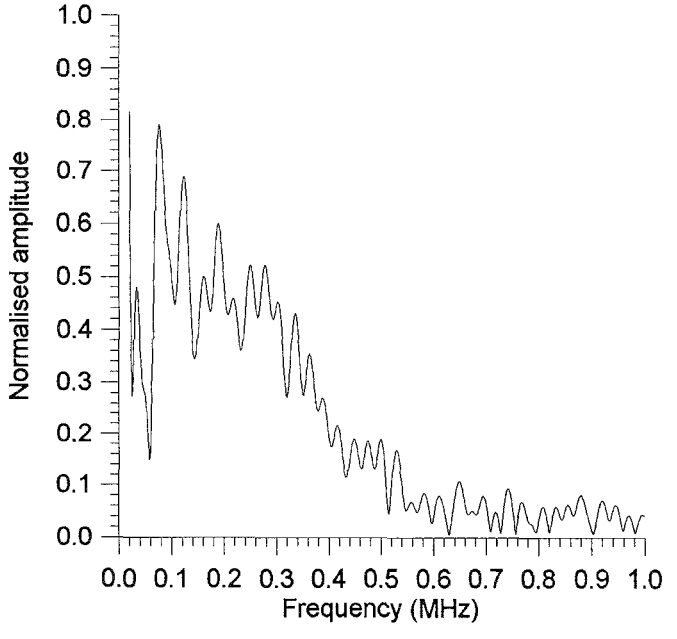

Figure 6(b)

Fig. 6. (a) A typical Lamb wave in 1 mm perspex (Plexiglas), obtained using the pair of air-coupled transducers. (b) The normalized frequency spectrum of Fig. 6(a).

defect was the shift in the centroid frequency f_C of a fast Fourier transform (FFT) of a waveform or ray, given by

$$f_C = \frac{\sum_{i=1}^{n} f_i \cdot a(f_i)}{\sum_{i=1}^{n} a(f_i)} \tag{3}$$

where n is the number of points in the FFT, f_i is the frequency at point i and $a(f_i)$ is the amplitude at frequency f_i.

IV. Results

A typical Lamb wave obtained using the pair of air coupled capacitance transducers is shown in Fig. 4(a) for a 0.69 mm aluminium sheet, with the normalized frequency spectrum of the signal shown in Fig. 4(b). The waveform is the result of 128 averages to improve the signal to noise ratio, and the characteristic a_0 dispersion is visible before the larger direct wave through the air. The images shown in Fig. 5 are for a recess 8 mm in diameter machined halfway through a 0.69 mm thick aluminium sheet, formed from (a) the signal amplitude (dB mm^{-1}), (b) the time of flight (slowness image in μs mm^{-1}) and (c) the shift in centroid frequency (kHz) as the measured parameter. The expected size, shape, and location of the defect in each image is shown by a dashed line, and the defect is clearly resolved despite diffraction effects, and the size of both source and receiver. Fig. 6(a) shows the Lamb wave obtained in a Perspex sheet 1 mm thick, with the corresponding normalized frequency spectrum in Fig. 6(b). Images were also obtained for a 5 mm diameter hole in the same material, as shown in Fig. 7 for (a) attenuation (dB mm^{-1}), (b) slowness (μs mm^{-1}), and (c) shift in centroid frequency (kHz). The elongated shape in Fig. 7(a) is due to the presence of cracks produced by the machining of the defect. Note also that despite the two distorted projections in Fig. 7(b), the defect image was still clearly reconstructed.

The image of a 10 mm diameter recess machined halfway through a 16-ply (2.2 mm nominal thickness) carbon fiber reinforced polymer (CFRP) composite plate is shown in Fig. 8 using the shift in centroid frequency (kHz), with the defect offset by 10 mm from the center of the scan in each direction. This was to show that the technique could also resolve non-central defects, as the projections are more widely separated towards the edge of the scan area.

To see if the technique could resolve strongly non circular defects, a 1 mm by 10 mm slot was machined through a 0.69 mm thick sheet of aluminium, and offset from the center by 10 mm in one direction. The scan size was increased to 60 mm, in 1 mm steps, to give 61 rays per projection. The resultant tomographic reconstruction is shown in Fig. 9 using (a) the signal amplitude (dB mm^{-1}), and (b) the shift in centroid frequency (kHz). The algorithm

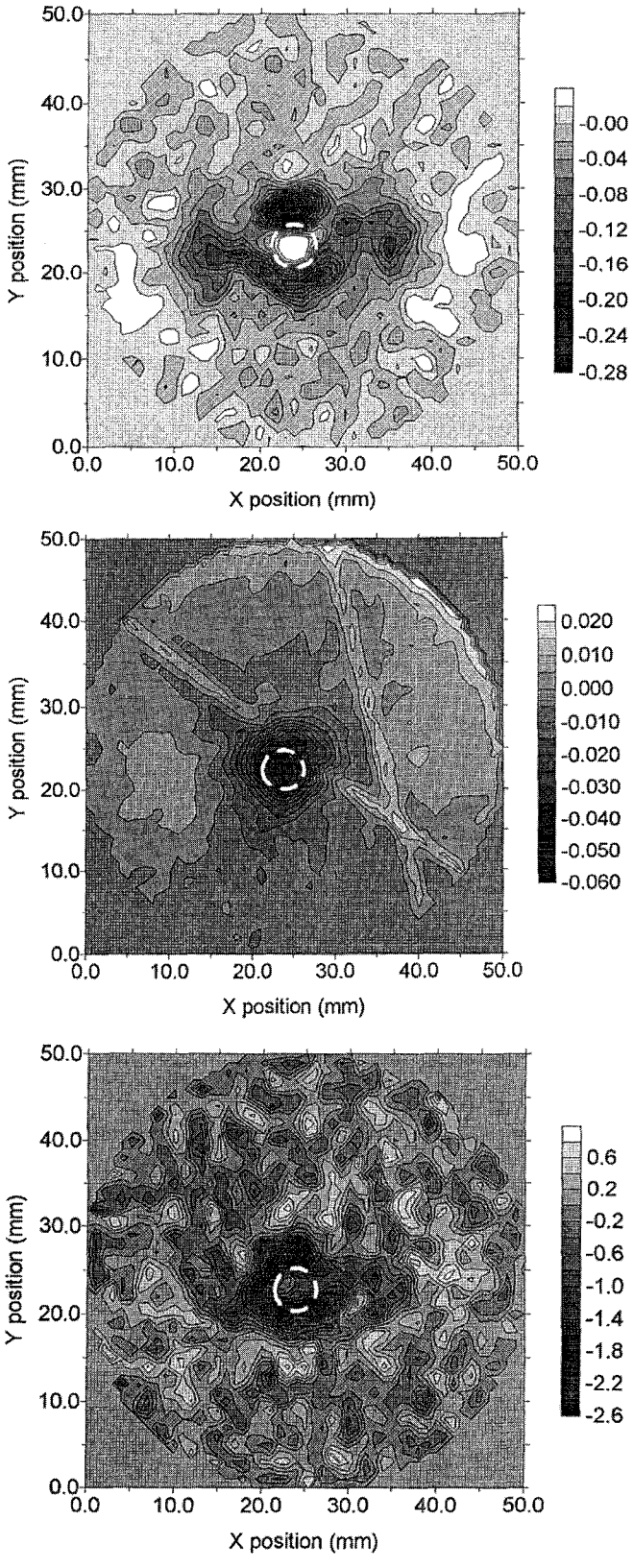

Fig. 7. (a) Attenuation image in dB mm^{-1} of a 5 mm hole through a 1 mm sheet of perspex (Plexiglas). (b) Slowness image in μs mm^{-1} of the 5 mm hole through a 1 mm sheet of perspex (Plexiglas). (c) Image of shift in centroid frequency in kHz of the 5 mm hole through a 1 mm sheet of perspex (Plexiglas).

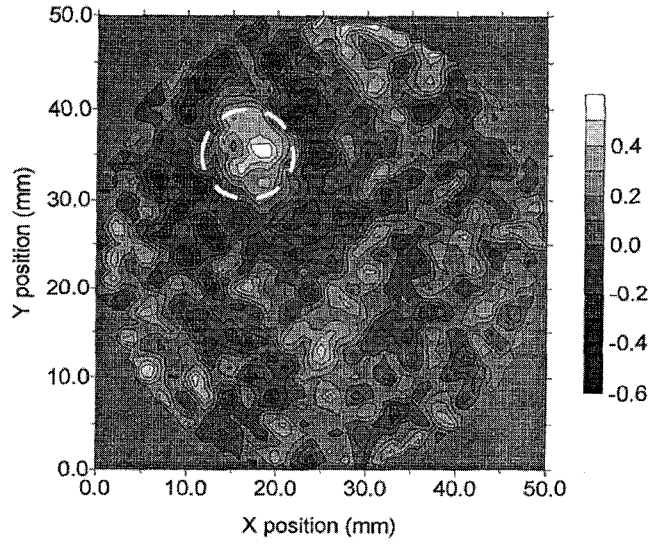

Fig. 8. Image in kHz of a 10 mm diameter recess in 16-ply (2.2 mm thick) cross-ply CFRP plate, using shift in centroid frequency.

did not reproduce the slot shape accurately, possibly due to the size of the defect in relation to the scan resolution and the ultrasonic wavelengths available, but it has picked out the diffraction at the ends of the slot in both images. To see if the technique could resolve more than one defect in the scan area, a 0.69 mm aluminium plate was machined with a 10 mm diameter hole in the center and a 5 mm diameter hole offset from the center by 20 mm in both X and Y directions. The resulting tomographic images are shown in Fig. 10(a) for the change in signal amplitude (dB mm^{-1}), and Fig. 10(b) for the shift in centroid frequency (kHz). In both cases, the two defects are resolved, with a greater change in signal amplitude or frequency shift associated with the larger defect. The location of the 5 mm defect is distorted due to the spacing of the projections at the edge of the scan area.

V. Conclusions

Ultrasonic tomographic imaging was performed using a pair of micromachined silicon air-coupled capacitance transducers and air-coupled Lamb waves. A difference technique and a filtered back projection algorithm were used to obtain images of various machined defects in thin plates of aluminium, perspex (or Plexiglas), and samples of carbon fiber reinforced polymer composite (CFRP) up to 2.2 mm thick. This flexible system produced images of the change in attenuation, velocity (using slowness), and shift in centroid frequency from one set of experimental data, with success dependent on the size, shape, and location of the defect within the scan area. The resolution of the system could be improved by using higher frequency devices with a broader bandwidth and a smaller spatial separation between each ray. The technique shows promise for future work.

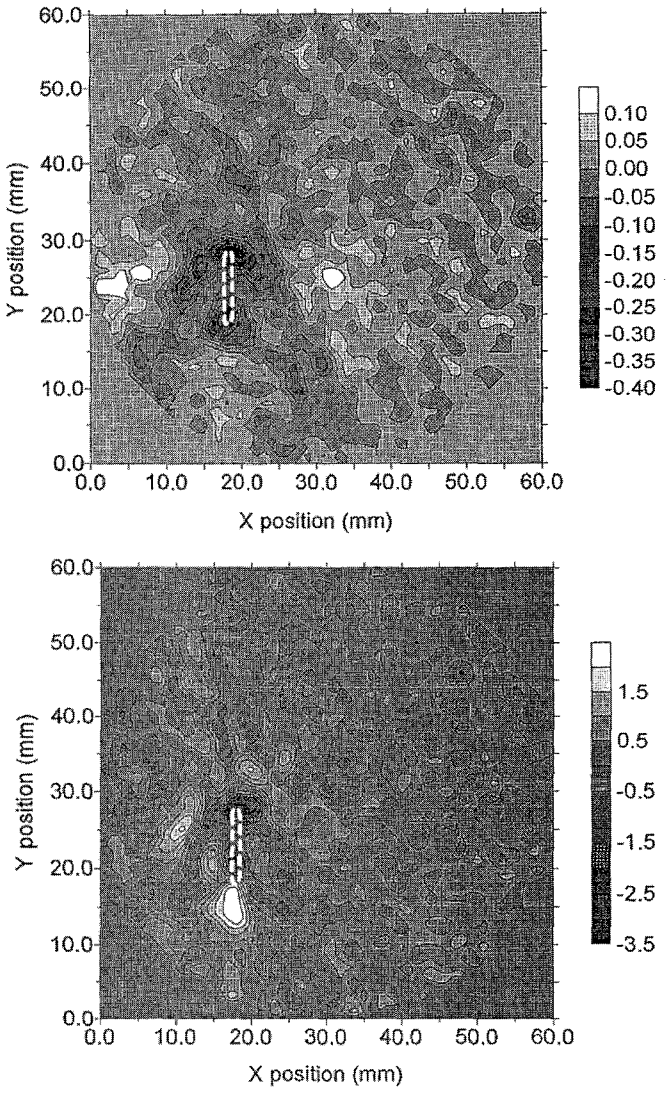

Fig. 9. (a) Attenuation image in dB mm^{-1} of a 1 mm by 10 mm slot in a 0.69 mm aluminium sheet, off-center by 10 mm in the horizontal direction. (b) Image of shift in centroid frequency in kHz of a 1 mm by 10 mm slot in a 0.69 mm aluminium sheet, off-center by 10 mm in the horizontal direction.

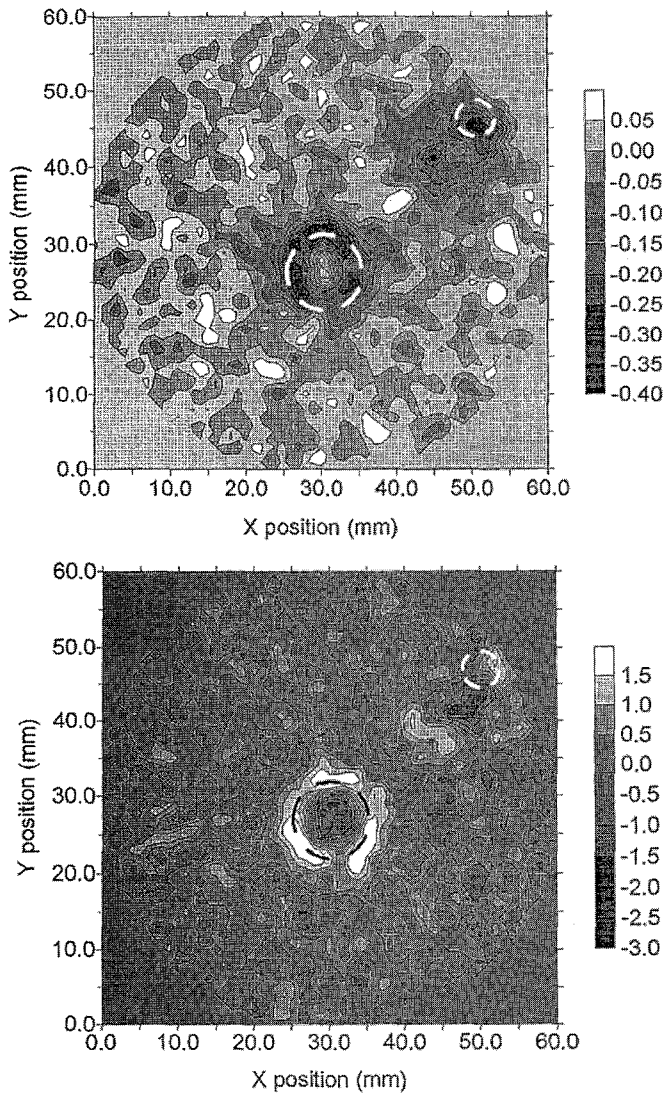

Fig. 10. (a) Attenuation image in dB mm^{-1} of a 10 mm hole (center) and a 5 mm hole (offset by 20 mm in both directions) through a 0.69 mm aluminium sheet. (b) Image of shift in centroid frequency in kHz of a 10 mm hole (center) and a 5 mm hole (offset by 20 mm in both directions) through a 0.69 mm aluminium sheet.

References

[1] A. C. Kak and M. Slaney, *Principles of Computerized Tomographic Imaging*, IEEE Press, New York, 1988.

[2] H. Yamada, "Application of ultrasonic computed tomography to non-destructive inspection of SiO_2 ingot", *J. Acoust. Soc. Am.*, vol. 69, pp. 571–572, 1978.

[3] A. M. H. Satti and J. Szilard, "Computerised ultrasonic tomography for testing solid propellant rocket motors," *Ultrasonics*, vol. 21, pp. 162–166, 1983.

[4] Y. Tomikawa, "Non-destructive inspection of wooden poles using ultrasonic computed tomography," *IEEE Trans. Ultrason., Ferroelect., Freq. Contr.*, vol. 33, pp. 354–358, 1986.

[5] D. P. Jansen, D. A. Hutchins, and R. P. Young, "Ultrasonic tomography using scanned contact transducers," *J. Acoust. Soc. Am.*, vol. 93, pp. 3242–3249, 1993.

[6] T. M. Chow, D. A. Hutchins, and J. T. Mottram, "Simultaneous acoustic emission and ultrasonic tomographic imaging in anisotropic polymer composite material," *J. Acoust. Soc. Am.*, vol. 94, pp. 944–953, 1993.

[7] T. Chow, D. A. Hutchins, M. D. C. Moles, and R. P. Young, "Stress dependence of the acoustic properties of Zr-2.5 wt% Nb alloy," *Ultrasonics*, vol. 31, pp. 183–192, 1993.

[8] D. A. Hutchins, J. K. Hu, R. P. Young, R. Stoner, D. Jansen, and Q. L. Zhang, "Ultrasonic tomography of metals using non-contact transduction," *J. Acoust. Soc. Am.*, vol. 85, pp. 747–752, 1989.

[9] D. A. Hutchins, D. P. Jansen, and C. Edwards, "Lamb-wave tomography using non-contact transduction," *Ultrasonics*, vol. 31, pp. 97–103, 1993.

[10] J. K. Hu, D. A. Hutchins, J. Ungar, Q. L. Zang, and D. K. Mak, "Non-contact ultrasonic reflection tomography," *Mat. Eval.*, vol. 47, pp. 736–740, 1987.

[11] D. P. Jansen, D. A. Hutchins, and J. T. Mottram, "Lamb wave tomography of advanced composite laminates containing damage," *Ultrasonics*, vol. 32, pp. 83–89, 1994.

[12] H. Carr and C. Wykes, "Diagnostic measurements in capacitive transducers," *Ultrasonics*, vol. 31, pp. 13–20, 1993.

[13] W. Manthey, N. Kroemer, and V. Mágori, "Ultrasonic transducers and transducer arrays for applications in air," *Meas. Sci. Technol.*, vol. 3, pp. 249–261, 1992.

[14] D. W. Schindel and D. A. Hutchins, "Air-coupled ultrasonic transducer," U.S. Patent S. N. #07/966,649, 1994.

[15] D. W. Schindel, D. A. Hutchins, L. Zou, and M. Sayer, "The design and characterization of micro-machined air-coupled capacitance transducers," *IEEE Trans. Ultrason., Ferroelect., Freq. Contr.*, vol. 42, pp. 42–50, 1995.
[16] Y. Censor, "Finite series expansion reconstruction techniques," *Proc. IEEE*, vol. 71, pp. 409–419, 1984.
[17] R. Gordon, R. Bender, and G. T. Herman, "Algebraic reconstruction techniques for three-dimensional electron microscopy and X-ray photography," *J. Theor. Biol.*, vol. 29, pp. 471–481, 1970.
[18] P. Gilbert, "Iterative methods for the three-dimensional reconstruction of an object from projections," *J. Theor. Biol.*, vol. 29, pp. 105–117, 1972.
[19] R. A. Kline and Y. Q. Wang, "A technique for ultrasonic tomography in anisotropic media," *J. Acoust. Soc. Am.*, vol. 91, pp. 878–884, 1992.
[20] R. M. Lewitt, "Reconstruction algorithms: transform methods," *Proc. IEEE*, vol. 71, pp. 390–408, 1984.
[21] H. H. Stark, J. W. Woods, I. Paul, and R. Hingorani, "Direct Fourier reconstruction in computer tomography," *IEEE Trans. Acoust., Speech, Sig. Proc.*, vol. 29, pp. 237–245, 1981.
[22] G. T. Herman, *Image Reconstruction from Projections: The Fundamentals of Computerized Tomography*, Academic Press, NY, 1980.
[23] D. P. Jansen and D. A. Hutchins, "Immersion tomography using Rayleigh and Lamb waves," *Ultrasonics*, vol. 30, pp. 245–254, 1992.
[24] L. Capineri, H. G. Tattersall, J. A. G. Temple, and M. G. Silk, "Time of flight diffraction tomography for NDT applications," *Ultrasonics*, vol. 30, pp. 275–288, 1992.
[25] A. J. Devaney, "A fast filtered backpropagation algorithm for ultrasound tomography," *IEEE Trans. Ultrason., Ferroelect., Freq. Contr.*, vol. 34, pp. 330–340, 1987.
[26] L. S. Koo, H. R. Shafiee, D. K. Hsu, S. J. Wormley, and D. O. Thompson, "Two-dimensional ultrasonic tomography in nondestructive evaluation by using area functions," *IEEE Trans. Ultrason., Ferroelect., Freq. Contr.*, vol. 37, pp. 148–158, 1990.

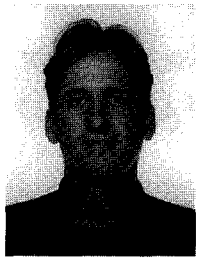

William Wright received his B.Eng. and Ph.D. in engineering from the University of Warwick, England in 1991 and 1996, respectively. He is currently employed as a Research Associate in the Department of Engineering, University of Warwick where his research interests include laser ultrasound, air-coupled transducers, and materials evaluation. He is a member of the Acoustical Society of America.

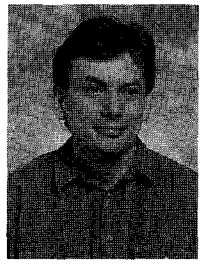

David Hutchins (M'81) received his B.Sc. and Ph.D. from the University of Aston, England in 1975 and 1979, respectively, before being employed on Postdoctoral fellowships in Denmark, England, and Canada. In 1982 he joined Queen's University in Canada as an Assistant Professor of Physics, and became an Associate Professor in 1985. In 1988 he returned to England at the University of Warwick, where he is now a Professor in Engineering. His research interests include ultrasonic transduction, imaging, and materials characterisation. Professor Hutchins is a member of the IEEE, the Acoustic Society of America, and the Institute of Physics.

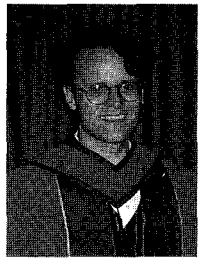

David Schindel received his B.Sc. and Ph.D. degrees in Engineering Physics from Queen's University, Canada in 1988 and 1995, respectively. His research interests to date have involved: measurement techniques for high temperature acoustics; acoustic thermometry; the development of capacitance transducers for solid, liquid, and gaseous media; and the application of micromachining to transducer and sensor design.

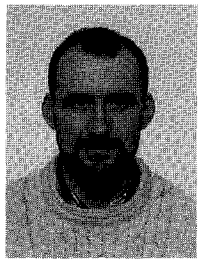

Dion Jansen received a B.Sc. in Engineering Physics from Queen's University at Kingston, Ontario in 1986. In 1992 he received his Ph.D. in Physics, also from Queen's, where his research interests included ultrasonic tomography for NDE and geophysical applications. He has been employed since 1992 as a research engineer in the Advanced Systems Technology group at Ontario Hydro Technologies in Toronto, Ontario. Current research interests include the ultrasonic NDE of steam generator tubing and piping.